JOURNAL OF BACTERIOLOGY, Apr. 2008, p. 2903–2910 Vol. 190, No. 8
0021-9193/08/$08.00+0 doi:10.1128/JB.01120-07

RhaU of *Rhizobium leguminosarum* Is a Rhamnose Mutarotase▽

Jason S. Richardson,[1] Xavi Carpena,[2] Jack Switala,[1] Rosa Perez-Luque,[2] Lynda J. Donald,[3] Peter C. Loewen,[1] and Ivan J. Oresnik[1]*

Department of Microbiology, University of Manitoba, Winnipeg, Manitoba R3T 2N2, Canada[1]; Departament de Biologia Estructural (IBMB-CSIC), Institut de Recerca Biomedica (IRB), Parc Científic de Barcelona, Josep Samitier 1-5, 08028 Barcelona, Spain[2]; and Department of Chemistry, University of Manitoba, Winnipeg, Manitoba R3T 2N2, Canada[3]

Received 16 July 2007/Accepted 11 December 2007

Of the nine genes comprising the L-rhamnose operon of *Rhizobium leguminosarum*, *rhaU* has not been assigned a function. The construction of a Δ*rhaU* strain revealed a growth phenotype that was slower than that of the wild-type strain, although the ultimate cell yields were equivalent. The transport of L-rhamnose into the cell and the rate of its phosphorylation were unaffected by the mutation. RhaU exhibits weak sequence similarity to the formerly hypothetical protein YiiL of *Escherichia coli* that has recently been characterized as an L-rhamnose mutarotase. To characterize RhaU further, a His-tagged variant of the protein was prepared and subjected to mass spectrometry analysis, confirming the subunit size and demonstrating its dimeric structure. After crystallization, the structure was refined to a 1.6-Å resolution to reveal a dimer in the asymmetric unit with a very similar structure to that of YiiL. Soaking a RhaU crystal with L-rhamnose resulted in the appearance of β-L-rhamnose in the active site.

Rhizobium leguminosarum bv. trifolii is a gram-negative soil bacterium that can form symbiotic associations with various species of clover. The plant provides the bacteria with energy for growth, and in return the bacteria provide the plant with fixed nitrogen from nitrogen-fixing nodules. Competition for nodule occupancy exists among strains of *Rhizobium* within the rhizosphere (10, 40), and strains of *R. leguminosarum* unable to catabolize L-rhamnose are compromised in their ability to compete for nodule occupancy (24).

L-Rhamnose is a 6-deoxyhexose monosaccharide found in the mucilage of a number of legume plants and is a constituent of pectin in the form of rhamnogalacturonan within the cell walls of dicotyledonous plants (17, 20). The 11-kb L-rhamnose locus in *R. leguminosarum* comprises L-rhamnose transport and catabolism genes (24, 28) organized in two divergently transcribed operons controlled by a negative regulator, *rhaR* (28). One transcript contains *rhaD* and *rhaI*, encoding a dehydrogenase/aldolase and an isomerase, respectively, while the other consists of *rhaRSTPQUK* (28). *rhaS*, *rhaT*, *rhaP*, and *rhaQ* encode the components of an ABC transporter, including a periplasmic sugar binding protein, an ABC ATPase, and two permeases, respectively (3). Within the L-rhamnose catabolic pathway, the enzymatic action of the kinase, encoded by *rhaK*, has been shown to precede the action of the dehydrogenase and the isomerase encoded by *rhaD* and *rhaI*, respectively (28). Moreover, the biochemical activity of the kinase appears to be necessary for L-rhamnose transport (29).

Among the nine genes in the operon, only *rhaU* does not have an assigned role, and database searches revealed a number of similar open reading frames, none of which had an assigned function. However, YiiL, originally annotated as a hypothetical protein from the *Escherichia coli* genome, has recently been shown to be an L-rhamnose mutarotase, providing a strong clue to the identity of RhaU. Mutarotases facilitate the interconversion of α and β anomers where the stereochemically less-favored anomer is required for a subsequent step in a catabolic sequence. Three such examples have so far been identified, including L-rhamnose mutarotase (YiiL in *E. coli*) (30, 31), galactose mutarotase (GalM) (5, 6, 8, 9, 14, 36, 37, 38, 39), and fucose mutarotase (FucU) (16, 30). In this report, we characterize *rhaU* from *R. leguminosarum* and provide evidence that is consistent with the hypothesis that RhaU is an L-rhamnose mutarotase.

MATERIALS AND METHODS

Bacterial strains and culture conditions. The bacterial strains and plasmids used and generated in this work are listed in Table 1. *R. leguminosarum* strain Rlt100 (original designation W14-2 [4]) and strains derived from this wild-type strain were routinely grown at 30°C on TY as a complex medium (7) and VMM (42), a defined medium, as previously described (28). Carbon sources were filter sterilized and added to defined media to a final concentration of 15 mM. When required, antibiotics were added to solid or liquid media at the following concentrations: tetracycline, either 10 μg ml^{-1} or 5 μg ml^{-1}; neomycin, 200 μg ml^{-1}; streptomycin, 200 μg ml^{-1}; gentamicin, either 15 μg ml^{-1} or 30 μg ml^{-1}; ampicillin, 100 μg ml^{-1}; and kanamycin, 50 μg ml^{-1}. Bacterial growth was monitored spectrophotometrically at 600 nm.

DNA manipulations, sequencing, and sequence analysis. Standard techniques were used for plasmid isolation, restriction enzyme digestion, ligation, transformation, and agarose gel electrophoresis (32, 33). Genomic DNA was isolated using a modified version of the protocol outlined by Meade et al. (21), as previously described (24). Sequencing was carried out by the University of Calgary Core DNA Services. Sequence data were analyzed using DNASIS (Hitachi Software Engineering Co., San Bruno, CA). Database searches were done using the BLASTX program (2).

Overexpression and purification of RhaU. To construct a gene encoding a His_6-tagged RhaU, the coding region was amplified and cloned into pRSETA (34) using BamHI and EcoRI restriction sites introduced within the primers such that *rhaU* was under the control of the T7 promoter and in frame with the N-terminal His_6 tag. The primers used in the PCR amplification were 5′-ATA**TGGATCC**GGAGATATGACATTGGAAAAACACGC and 5′-ATAT**GAATT**

* Corresponding author. Mailing address: Department of Microbiology, University of Manitoba, Winnipeg, MB R3T 2N2, Canada. Phone: (204) 474-7587. Fax: (204) 474-7603. E-mail: oresniki@cc.umanitoba.ca.

▽ Published ahead of print on 21 December 2007.

TABLE 1. Bacterial strains and plasmids used in this study

Strain or plasmid	Genotype or phenotype[a]	Reference or source
Strains		
R. leguminosarum		
Rlt100	W14-2, *R. leguminosarum* bv. trifolii, Sm^r wild type	4
Rlt100/pMR110	Wild type carrying *rhaK* coding sequence in pRK7813	29
Rlt105	Rlt100 *rhaD1*::Tn*5*B20	24
Rlt144	Rlt100 *rhaK50*::Tn5B20	28
Rlt144/pMR110	Rlt100 *rhaK50*::Tn5B20 carrying *rhaK* coding sequence in pRK7813	29
Rlt146	Rlt100 *rhaK52*::Tn5B20	28
Rlt211	Rlt105 *rhaK58*::pKNOCK-Tc	28
Rlt218	Rlt100 *rhaU*::pJQ200 SK$^+$ single crossover	This work
Rlt218/pMR110	Rlt100 *rhaU*::pJQ200 SK$^+$ pMR174 single crossover carrying *rhaK* coding sequence in pRK7813	This work
Rlt243	Rlt100 Δ*rhaU*	This work
Rlt243/pMR110	Rlt100 Δ*rhaU* carrying *rhaK* coding sequence in pRK7813	This work
Rlt243/pMR183	Rlt100 Δ*rhaU* carrying *rhaU* coding sequence in pRK7813	This work
Rlt243/pW3C1	Rlt100 Δ*rhaU* cosmid from Rlt100 wild-type cosmid, containing entire L-rhamnose locus	This work
E. coli		
MT616	MT607/pRK600	24
DH5α	*endA hsdR17 supE44 thi-1 recA1 gyrA96 relA1* Δ(*argF-lacZYA*)*U169* ϕ80d*lacZ*Δ*M15*	BRL
Plasmids		
pBlueScript II SK	Cloning vector, ColE1 *oriV* Ap^r	Stratagene
pRK600	pRK2013 *npt*::Tn*9* Cm^r Nm-Km^s	24
pRK7813	RK2 *ori*, pUC9 polylinker, lambda *cos* site, Tc^r	15
pRSETA	N-terminal His_6 tag, T7 promoter, Ap^r	Invitrogen
pW3C1	pRK7813 cosmid from Rlt100 wild-type cosmid bank, containing entire L-rhamnose locus	24
pJQ200 SK$^+$	Suicide vector for homogenotization; P15a *ori mob sacB*, Gm^r	27
pMR110	*rhaK* coding sequence in pRK7813	29
pMR113	*rhaU* coding sequence in pRK7813	This work
pMR133	*rhaU* coding sequence in pRSETA	This work
pMR174	Δ*rhaU* flanking sequence in pJQ200 SK$^+$	This work

[a] Ap, ampicillin; Cm, chloramphenicol; Gm, gentamicin; Km, kanamycin; Nm, neomycin; Sm, streptomycin; Tc, tetracycline.

CTCATGGCATATGGAAGAGG (bold type indicates restriction sites). The sequence of the resulting construct, pMR133, was confirmed. For protein expression, pMR133 was transformed into *E. coli* BL21(DE3) (22), grown to mid-log phase (optical density at 600, 0.5), and induced with 1 mM IPTG (isopropyl-β-D-thiogalactopyranoside) at 37°C for 4 h. For selenium methionine (SeM) labeling, cultures were grown in M9 minimal medium supplemented with SeM at the time of induction. Cells were harvested, resuspended in buffer A (20 mM Tris [pH 7.8], 300 mM NaCl, 5 mM β-mercaptoethanol) supplemented with 10 mM imidazole, and lysed by two passages through a French pressure cell (16,000 lb/in^2). Cell extracts were passed through a nickel affinity column to bind the His_6-RhaU, and after the extracts were washed with buffer A plus 20 mM imidazole for 60 min, RhaU was eluted with 250 mM imidazole in buffer A. Protein samples were analyzed by sodium dodecyl sulfate (SDS)-polyacrylamide gel electrophoresis (19) and transferred to a nitrocellulose membrane for Western blot analysis by using a His_6 monoclonal antibody as a primary antibody and a goat anti-mouse secondary antibody conjugated with horseradish peroxidase antibody. Horseradish peroxidase was detected colorimetrically with an Opti-4CN substrate detection kit (Bio-Rad Laboratories).

Generation of the Δ*rhaU* strain. The Δ*rhaU* strain was constructed using the overlap extension PCR method (32), with pW3C1 as a template. The primers used were 5′-AA**GGATCC**GGTCAGGGCTATGTCGTC and 5′-AA**CTGCAG** GCAGCCGAGAGAGGTCAA, with the mutagenic primers 5′-TGGCGGTCA TCGGGAGCTCATGAGCTTG and 5′-TGAGCTCCCGATGACCGCCAGTT CCTATC (bold type indicates BamHI and PstI sites). The amplification product was cloned as a BamHI/PstI fragment into pJQ200SK (27) to generate pMR174. The gene replacement of *rhaU* in Rlt100 with pMR174 (Δ*rhaU*) was carried out as previously described (27) to generate strain Rlt243. The deletion of *rhaU* from strain Rlt243 was verified by sequencing (Fig. 1).

Transport assays. The uptake of L-rhamnose was carried out as described previously (28) using [^{3}H]L-rhamnose (5 Ci/mmol) (American Radiolabeled Chemicals, Ltd.). Transport assays were initiated by the addition of [^{3}H]L-rhamnose to a final concentration of 2 μM (125,000 dpm), and aliquots of 0.5 ml were removed, rapidly filtered through a Millipore 0.45-μm HV filter, and washed with 5 ml of the defined salts medium. The ^{3}H on the filters was quantified by liquid scintillation counting.

In vitro RhaK assays. Cultures were grown on minimal medium to mid-log phase, harvested by centrifugation, resuspended, and lysed by two passages through a French pressure cell. After the removal of cell debris, the cell extracts were mixed with 50 mM HEPES buffer (pH 7.6), 5 mM $MgCl_2$, 10 mM ATP, and 2 mM [^{3}H]L-rhamnose to a volume of 100 μl, from which aliquots were removed and boiled for 10 min. Samples were spotted on Whatman DE 81 cellulose chromatography paper that had been previously washed sequentially with 1 M formic acid and water to remove any impurities and then dried. After descending chromatography was done with 50 mM formic acid (pH 3.2), the paper was cut into 1-in.-square pieces and assayed using a liquid scintillation counter.

Crystallization and structure determination. The His tag-labeled RhaU was crystallized at room temperature by using the vapor diffusion hanging-drop method at a protein concentration of about 6 mg/ml over a reservoir containing 2 M sodium formate, 0.1 M sodium citrate (pH 5.6), and 20% glycerol. The crystallization buffer was supplemented with 10 mM L-rhamnose for a 1-min soaking. Crystals were trigonal, space group $P3_212$, with two subunits in the crystal asymmetric unit. Diffraction data were obtained from cryocooled crystals, giving the following unit cell parameters: a = 69.2 Å, b = 69.2 Å, c = 101.1 Å, α and β = 90.0°, and γ = 120.0°. A multiwavelength anomalous diffraction experiment was initially performed with a SeM derivative crystal. The heavy metal substructure was finally solved by the single-wavelength anomalous dif-

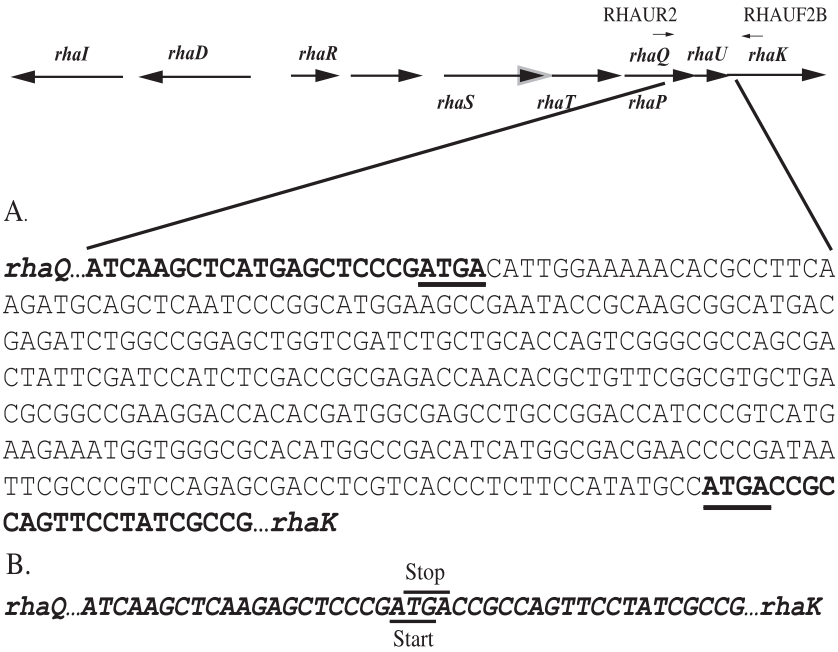

FIG. 1. Sequence of the wild type (Rlt100 *rhaQUK*) (A) and a *rhaU* deletion strain (Rlt243) (B) generated by site-specific mutagenesis by overlap extension PCR. The sequences corresponding to *rhaQ* and *rhaK* are bold and italicized. The *rhaQ* termination site and the *rhaK* initiation site that overlap the *rhaU* initiation and termination sites, respectively, are underlined in panels A and B. A schematic representation of the L-rhamnose catabolic operon is shown above panel A, with the corresponding flanking primers, RHAUR2 and RHAUF2B, used for sequencing.

fraction method using only the remote wavelength data set due to problems in data collection. The substructure of 15 selenium sites, solved by using SHELXD (41) through the graphic interface HKL2MAP (25), showed a correlation between observed and calculated E values of 44.28 (all data) and 22.41 (weak data). Phases were calculated and refined with SHELXE (35) by using all 15 selenium sites and using the slightly higher resolution peak data set. Two SHELXE jobs were started for the two possible enantiomorphs. The contrast and connectivity figures of merit for the correct solution were 0.680 and 0.937, respectively, and the pseudo-free correlation coefficient was 74%, well above the figures of merit for the wrong hand. Automatic model building performed with ARP/wARP (26) traced almost 100% of the asymmetric unit. Model rebuilding was carried out with Coot software (11), and refinement was effected using the REFMAC program (23). Refinement statistics are given in Table 2. All figures were prepared using the PyMOL molecular graphics system (W. L. DeLano; http://www.pymol.org).

Protein structure accession numbers. Structure factors and coordinates have been submitted to the Protein Data Bank under accession numbers 2QLW (native) and 2QLX (with L-rhamnose).

RESULTS

Generation of the Δ*rhaU* strain Rlt243. Previous random transposon mutagenesis of the *R. leguminosarum* L-rhamnose catabolic locus yielded a total of 56 independent mutants, none of which provided a lesion within *rhaU* (28). In order to determine if the product of *rhaU* was required for growth on or the transport of L-rhamnose, site-specific mutagenesis by overlap extension PCR (32) was used to generate the *rhaU* deletion strain, Rlt243. Nucleotide sequencing of the *rhaQ-rhaK* region in Rlt243 confirmed that no inadvertent mutations had been introduced and that the predicted upstream *rhaQ* termination site and predicted downstream *rhaK* start site were not interrupted (Fig. 1).

Rlt243 exhibits a slow-growth phenotype on L-rhamnose. Sequence similarity (41% identity) suggested that RhaU was related to a group of hypothetical proteins that included YiiL of *E. coli* (28), which was recently characterized as an L-rhamnose mutarotase, catalyzing the α- to β-anomeric conversion of L-rhamnose (30, 31). Based on the phenotype produced by *yiiL* in *E. coli*, it was expected that a *rhaU*-containing mutant would grow normally at high concentrations of L-rhamnose (0.2%) and more slowly at low concentrations (0.03%), but Rlt243 exhibited a slow-growth phenotype even at high L-rhamnose concentrations (Table 3). The mean growth rates for Rlt243 and Rlt100 were 0.0563 and 0.109 generations per hour, respectively (Fig. 2). Despite the low growth rate, the ultimate cell yields of Rlt243 and wild-type Rlt100 were indistinguishable, indicating that carbon utilization and final growth potential were not affected. To ensure that the slow-growth phenotype of Rlt243 was unique to L-rhamnose catabolism and not the result of a pleiotropic effect causing a generalized slow-growth potential, Rlt243 and Rlt100 were grown on a complex medium (TY) and VMM-glucose, with no discernible differences in growth rate or yield. Furthermore, identical slow-growth phenotypes were observed after every round of repeated streaking on VMM-rhamnose, confirming that the phenotype was not a result of the up-regulation of some uncharacterized L-rhamnose catabolic genes or the presence of a second site mutation. Plasmid pW3C1 bearing wild-type *rhaU* complemented the slow-growth phenotype, confirming that the slow-growth phenotype in Rlt243 was a result of Δ*rhaU* (Table 3).

Placement of RhaU in a biochemical pathway. RhaU would most reasonably be situated in a metabolic pathway to catalyze anomerization after transport into the cell prior to phosphorylation. A biochemical lesion in a catabolic pathway following

TABLE 2. Data collection, phasing, and structural refinement statistics for an RhaU SeM derivative and an L-rhamnose-soaked crystal

Statistic or parameter[a]	Result for[b]:	
	Remote-wavelength derivative	Soaked crystal
Data collection statistics for unit cell parameters		
Space group	$P3_212$	$P3_212$
a (Å)30–1.6 (1.66–1.60)	69.2	68.7
b (Å)	69.2	68.7
c (Å)	101.1	100.7
α, β, γ (degree)	90, 90, 120	90, 90, 120
Wavelength	0.9079	0.9330
Resolution (Å)	30–1.6 (1.66–1.60)	30–1.85 (1.92–1.85)
No. of unique reflections	35,978 (3,574)	23,317 (2,169)
Completeness (%)	97.1 (97.0)	98.3 (92.5)
R_{sym} (%)	9.7 (57.6)	9.1 (30.7)
$<I/\sigma I>$	11.0 (3.2)	8.0 (3.7)
Redundancy	5.7 (5.6)	4.2 (2.8)
Model refinement statistics for:		
Resolution	20–1.6 (1.64–1.60)	29–2.00 (2.05–2.00)
No. of reflections	33,997 (2,483)	17,475 (1,281)
No. of free reflections	1,786 (118)	942 (64)
R_{cryst} (%)	15.2 (21.3)	14.4 (14.8)
R_{free} (%)	18.0 (27.2)	19.1 (23.6)
No. of residues	1,428	216
No. of water molecules	220	204
Avg B factor (Å^2)		
Protein	12.7	19.9
Water	27.4	33.0
All atoms	17.3	21.9
RMSD		
Bond length (Å)	0.018	0.013
Bond angle (degree)	1.69	1.43

[a] $R_{sym} = \Sigma_{hkl} \Sigma_j |I_{hkl,j} - <I_{hkl}>| / \Sigma_{hkl} <I_{hkl}>$, where *j* extends to all the observed *hkl* symmetry-related reflections. $R_{cryst} = \Sigma ||F_{obs}| - |F_{calc}|| / \Sigma |F_{obs}|$. R_{free} is as for R_{cryst} but calculated for a test set comprising reflections not used for the refinement.

[b] Values in parentheses correspond with the highest-resolution shell.

the synthesis of a phosphorylated sugar intermediate can give rise to a conditional phenotype if the bacterium is grown on a medium that contains a noninducing carbon source that can be catabolized (1). For example, the conditional phenotype of the *rhaD*- and *rhaI*-containing Rlt105 was relieved by the introduction of a *rhaK* mutation in Rlt211, demonstrating that the action of RhaK occurs prior to RhaD and RhaI functions in *R. leguminosarum* (28). Rlt243 grew at wild-type levels on glycerol-rhamnose plates, implying that RhaU enzymatic action occurs before L-rhamnose phosphorylation (Table 3). However, a *rhaU*-containing strain may simply have been less sensitive to the accumulation of phosphorylated L-rhamnose intermediates. To test this possibility, RhaK levels were increased by introducing a *rhaK*-bearing plasmid into the *rhaU* deletion strain. The fact that even this RhaK-overproducing strain, Rlt243/pMR110, did not exhibit a conditional phenotype is consistent with RhaU working prior to RhaK in the catabolic pathway. Interestingly, the overexpressed RhaK had the unexpected effect of eliminating the slow-growth phenotype on VMM–L-rhamnose (Table 3).

TABLE 3. Strain growth on glucose, L-rhamnose, and glycerol-rhamnose

Strain	Genotype	Growth on[a]:		
		Glycerol	Glycerol-rhamnose	Rhamnose
Rlt100	Wild type	+	+	+
Rlt105	*rhaDI*	+	−	−
Rlt144	*rhaK*	+	+	−
Rlt144/pMR110	*rhaK rhaK*$^+$	+	+	+
Rlt211	*rhaDI rhaK*	+	+	−
Rlt243	Δ*rhaU*	+	+	±
Rlt243/pMR110	Δ*rha rhaK*$^+$	+	+	+
Rlt243/pW3C1	Δ*rhaU rha* locus$^+$	+	+	+

[a] +, similar to wild-type growth; −, no growth; ±, slower growth compared to that of Rlt100. A 15 mM concentration of each carbon source was added to defined medium (VMM).

***rhaU* is not necessary for the uptake or phosphorylation of L-rhamnose.** Since the slow-growth phenotype of the *rhaU* deletion strain Rlt243 was complemented by plasmid-borne wild-type *rhaK*, RhaK-dependent L-rhamnose phosphorylation and transport levels were investigated. Transport rates in Rlt100 (wild type), Rlt243 (Δ*rhaU*), and Rlt243/pWC3C1 (Δ*rhaU* complemented with *rhaU*) were similar (Table 4), suggesting that the uptake of L-rhamnose was normal in the absence of RhaU and that extra copies of RhaU did not enhance uptake. In contrast, transport in the *rhaK* mutant strain, Rlt144, was undetectable but could be rescued by the plasmid-borne *rhaK* in Rlt144/pMR110 (data not shown). Rhamnose phosphorylation levels were unaffected by the Δ*rhaU* mutation in Rlt243 compared to that of wild-type Rlt100 (Table 5), and

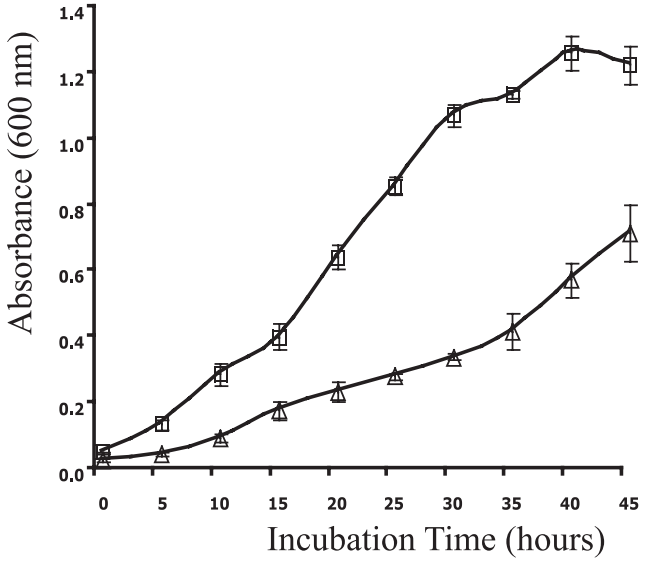

FIG. 2. Growth curves of *R. leguminosarum* wild-type (Rlt100) and *rhaU* deletion (Rlt243) strains based on absorbance measured at a wavelength of 600 nm. Strains were grown on minimal medium supplemented with 15 mM L-rhamnose as the sole carbon source. Squares, Rlt100; triangles, Rlt243.

TABLE 4. Transport of [^{3}H]L-rhamnose

Strain	Relevant genotype	[^{3}H]L-rhamnose transported (nmol/gfw/min)[a]
Rlt100	Wild type	30.7 ± 1
Rlt100/pMR110	Wild type *rhaK*$^+$	24.7 ± 6.6
Rlt243	Δ*rhaU*	36.9 ± 6.4
Rlt243/pMR110	Δ*rhaU rhaK*$^+$	28.3 ± 6.7
Rlt243/pW3C1	Δ*rhaU rha*$^+$	28.5 ± 4.5
Rlt144	*rhaK*	<0.05

[a] Strains were grown as broth cultures in minimal medium (VMM) supplemented with 15 mM L-rhamnose–glycerol. Initial transport rates were determined using tritiated L-rhamnose. The data are presented as the means ± standard deviations (n = 3). gfw, grams (fresh weight).

the RhaK-bearing plasmid pMR110 did not significantly enhance the amount of phosphorylation (Table 5) or increase L-rhamnose transport (Table 4).

RhaU overexpression and purification. To investigate further the role that RhaU has in L-rhamnose catabolism in *R. leguminosarum*, a biochemical approach was initiated. Since the nearest homologue to *rhaU* was annotated as a hypothetical open reading frame, the first step was to demonstrate that *rhaU* encoded an expressible protein. An in-frame, His_6-tagged version of *rhaU* under the control of a T7 promoter was constructed in the plasmid pMR133, and the protein was purified on a nickel affinity column containing a mixture of three proteins, all of which cross-reacted with monoclonal antibodies to the RGS-His_6 tag in a Western blot (Fig. 3). The lower two bands migrated with apparent masses of 12,000 and 14,000 Da, while the smaller upper band appeared to be a dimer with a mass of approximately 28,000 Da. Because the sizes of the lower two bands were smaller than the predicted 16,595 Da, the protein was analyzed by mass spectrometry, confirming a deconvoluted monomer size of 16,593 Da and providing no evidence of a second protein (Fig. 4, inset A). The mass spectrum of RhaU also revealed that RhaU existed predominantly as a dimer and that increasing ionization voltage caused its dissociation to a monomer (Fig. 4). While it is possible that the dimer is due to different charge states of the protein due to partial decarboxylations of the glutamic acid residues, we do not have a definitive explanation for the existence of the two bands of protein on the SDS gel.

Crystal structure of RhaU. Attempts to solve the structure of RhaU by molecular replacement using the YiiL structure were not successful. However, a solution was found using mul-

TABLE 5. Rate of L-rhamnose phosphorylation[a]

Strain	Relevant genotype	Activity (μmol/min/mg)
Rlt100	Wild type	426
Rlt100/pMR110	Wild type *rhaK*$^+$	300
Rlt146	*rhaK*52	12
Rlt243	Δ*rhaU*	382
Rlt243/pMR110	Δ*rhaU rhaK*$^+$	461
Rlt243/pW3C1	Δ*rhaU rha*$^+$	479

[a] Strains were grown in minimal medium (VMM) supplemented with 15 mM L-rhamnose–glycerol; induced cell extract was isolated and processed as described in Materials and Methods. Values are presented as one representative set of data. Data are the average of two independent replicates.

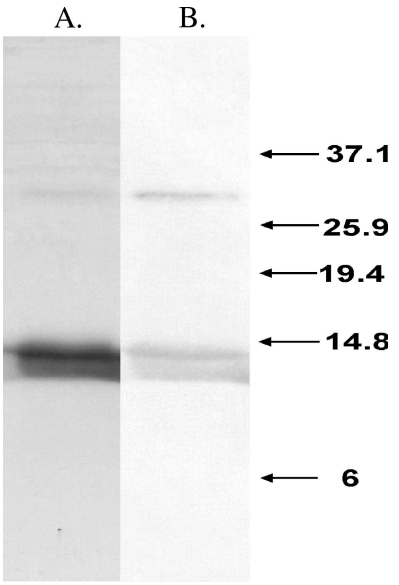

FIG. 3. A 15% SDS-polyacrylamide gel stained with Coomassie blue (A) and an associated Western blot (B) of purified His-tagged RhaU. The numbers indicate in kDa the locations of Invitrogen benchmark prestained ladder proteins run as size markers.

tiple-wavelength anomalous scattering from a crystal containing SeM. Mass spectrometry analysis of the His tag-labeled protein revealed approximately 70% replacement of sulfur by selenium (Fig. 4, inset B), but this was clearly sufficient sele-

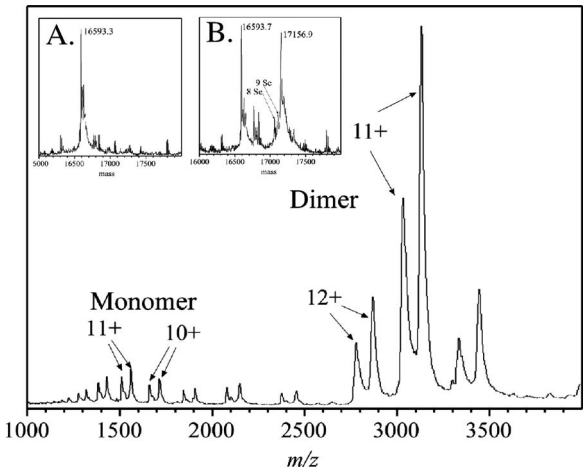

FIG. 4. Electrospray mass spectrometry analysis of RhaU protein prepared from medium containing methionine or SeM. After purification, the proteins were dialyzed into 5 mM ammonium acetate, diluted to approximately 10 μM, and sprayed directly into a 16-kV time-of-flight instrument at the Department of Physics and Astronomy, University of Manitoba (18). Part of the spectrum from the SeM protein was obtained at a 110-V spray voltage, where most of the ions are from the folded species of protein. Each of the two ion envelopes shows pairs of ions from monomers at 1,500 m/z, as shown in panel B, and from dimers at 3,000 m/z. Inset A, deconvolutions of spectra obtained at a 250-V spray voltage for the methionine-containing protein; inset B, the SeM-containing protein showing ions with 10, 9, and 8 SeM substitutions. Unlabeled ions are from residual buffer salts. At this voltage, most of the ions were unfolded monomers.

nium for phase determination. The mass of the Se-labeled RhaU was 17,157 Da compared to a predicted mass of 17,158 Da (Fig. 4). Only two sorts of dimers are evident. One contains exclusively methionine and must have been synthesized prior to the shift to SeM medium; the second type contains only SeM and must have been synthesized after the medium change. Some of the latter have less than the 10 expected substitutions, which is reasonable if there was residual methionine in the culture medium. From the relative peak areas, the relative incorporation of SeM for the total protein preparation was about 60%. The electron density map defines main chain and side chain atoms of 216 amino acids in two subunits and 220 water molecules. The maps show clear continuity in both subunits over the complete length from Met1 to Pro106. Of the predicted 38 residues in the His tag sequence at the N terminus, only Gly1 and Asp0 were clearly visible and the remaining 36 residues were presumably disordered. The model has crystallographic agreement R_{cryst} and R_{free} factors of 15.2 and 18.0% for 33,997 reflections in the resolution shell between 1.6 and 20 Å. The average root mean square deviation (RMSD) after the superimposition of the two subunits is 0.26 Å for the Cα atoms and 0.41 Å for all atoms. Ramachandran plots confirm that all residues lie within the energetically favorable regions in both subunits. Based on coordination geometry and electron density, a single metal ion assigned as Mg was associated with C═O of Ala83, the C═O of Met86, and Oγ of Thr88 on the surfaces of both subunits, something that was not observed in YiiL. This is 10 Å from the L-rhamnose binding site and is not affected by L-rhamnose binding.

Despite the lack of success in using the YiiL structure as a probe for a molecular replacement structural solution, the structures of YiiL and RhaU are very similar, with an RMSD after the superimposition of 1.01 and 0.98 Å for the Cα atoms in subunits A and B, respectively, when the subunits were superimposed separately. The RMSD increased to 1.56 Å when the subunits were superimposed simultaneously, indicative of a slightly different orientation of the two subunits in the dimer between the two enzymes. The only significant deviation of the main chains lies between residues 60 and 62 at the transition between β-strand 3 and a short α-helical section where the RMSD increases to >4 Å. Like YiiL, a single subunit is comprised of four long β strands in an antiparallel organization that form the interface with the second subunit in the dimer and three α-helical sections that form a cage with the β sheets to house the active site (Fig. 5).

Unlike YiiL, RhaU crystallizes without L-rhamnose bound in the active site, thereby providing an opportunity to study structural changes arising from substrate binding. Soaking RhaU crystals with L-rhamnose results in the appearance of new electron density in the central cavity adjacent to His24 that can be modeled satisfactorily as β-L-rhamnose (Fig. 6B). In subunit B, where the L-rhamnose bound with near 100% occupancy, each of its oxygen atoms forms a hydrogen bond with the protein, including O(H)-1 with Tyr20, OH-2 through water molecules O30 and O94 to the main chain C═O of Trp79 and Asn92, OH-3 with Trp79 and through water molecule O194 with Gln96, OH-4 with Tyr43, and the ring oxygen O-5 with the imidazole of His24 and the indole of Trp78. The C-6 methyl group falls in a relatively hydrophobic pocket composed of Ile27 (3.9 Å), Leu35 (4.12 Å), Leu31 (4.25 Å), and Phe103 (4.44 Å). Omit maps reveal that two water molecules from the native structure (Fig. 6A) are replaced by L-rhamnose, including U-10 by OH-1 and U-11 by ring O-5 (where U indicates a water molecule present when rhamnose was unbound). In addition, water molecule O194 is displaced by 2.3 Å by OH-3, and water molecule O195 is displaced 2.5 Å by OH-4. The only portion of the protein that changes as a result of L-rhamnose binding is the indole ring of Trp79, which is shifted almost 1 Å in order for it to interact with OH-3 of the L-rhamnose. In subunit A, there is an estimated 60% occupancy of L-rhamnose, with a corresponding overlap of L-rhamnose and native water molecules.

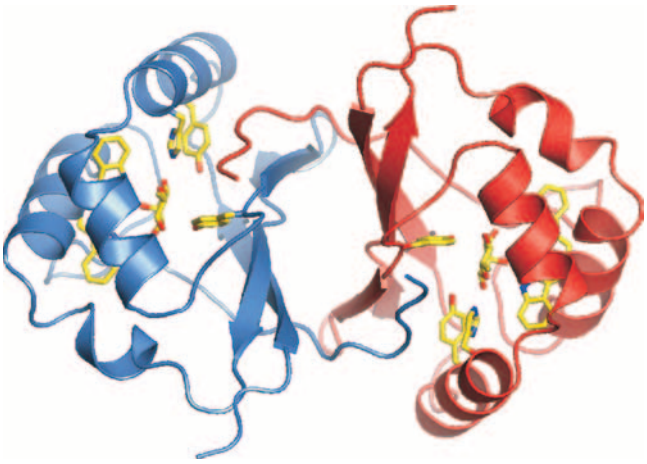

FIG. 5. View of RhaU to illustrate the relationship of the subunits, the location of rhamnose binding sites in the dimer, and the orientation of the key binding residues. Subunit A is blue, and subunit B is red.

DISCUSSION

The primary phenotype exhibited by the *R. leguminosarum* Δ*rhaU* strain is a lower growth rate than that of the wild-type strain but one that ultimately leads to the same growth yield as the wild type's. The phenotype is consistent with the L-rhamnose mutarotase activity ascribed to RhaU, which would be expected to speed up L-rhamnose catabolism but not be essential. In contrast to *E. coli*, in which the slow-growth phenotype of a *yiiL*-containing mutant strain was observed only at low L-rhamnose concentrations, the slow-growth phenotype of a *rhaU*-containing mutant strain was evident even at high L-rhamnose concentrations. The fact that elevated RhaK levels mask the slow-growth phenotype of the *R. leguminosarum rhaU* mutant at high L-rhamnose concentrations suggests that the discrepancy with the *E. coli yiiL* mutant may lie in RhaK levels in *R. leguminosarum* that are lower than the RhaA/RhaB levels in *E. coli*. Thus, the uncatalyzed α- to β-anomeric conversion is sufficient to support a low rate of growth in *R. leguminosarum*, and the role of RhaU is to facilitate the anomerization, thereby allowing a higher rate of growth. Indeed, the equilibrium ratio of α and β anomers in L-rhamnose, determined by nuclear magnetic resonance analysis to be 56:44 (31), suggests a relatively low energy barrier for α to β anomerization of approximately 0.15 to 0.2 kcal/mol, and displacement of the α ⇋ β

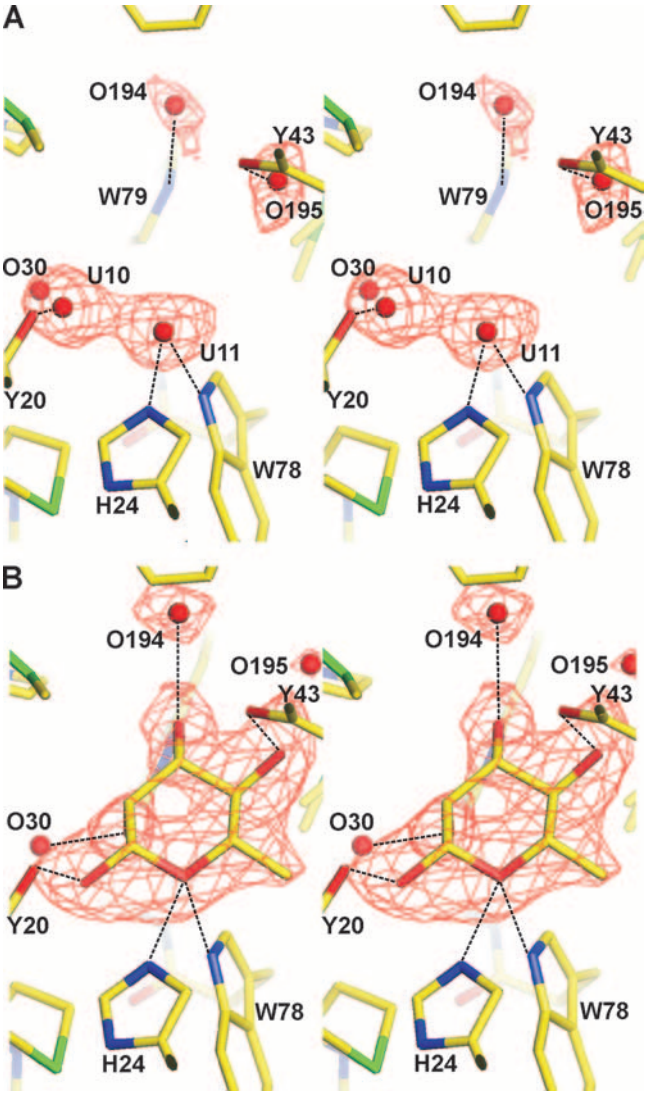

FIG. 6. Stereoview omit F_{obs}-F_{calc} electron density maps of the rhamnose binding site on RhaU. The maps were calculated with no water molecules or rhamnose in the binding site. (A) The omit map of the native protein prior to rhamnose binding. The red spheres indicate the water molecules that were ultimately refined into the model. (B) The omit map calculated after rhamnose binding. A model of rhamnose is superimposed on the map in the location where it was subsequently refined. In both panels, the F_{obs}-F_{calc} density shown in red is modeled at a σ of 3.0.

anomerization equilibrium by the phosphorylation of the β anomer or a subsequent metabolite is not unexpected.

Three possibilities exist for the position at which RhaU might function in the L-rhamnose catabolic pathway. The first is in the periplasm prior to transport, but RhaU is phylogenetically unrelated to other periplasmic mutarotases like GalM of *Acinetobacter calcoaceticus* (9, 12, 13), and RhaU does not contain a leader targeting sequence. The other two options have RhaU functioning either before or after RhaK-dependent phosphorylation, and differentiation is complicated by the requirement of RhaK for both transport and phosphorylation (29). If RhaU functions before phosphorylation, as in the *E. coli* L-rhamnose catabolism pathway, RhaK will have to function in two steps separated by the RhaU mutarotation step. On the other hand, the placement of RhaU following phosphorylation would allow RhaK to carry out transport and phosphorylation as part of the same step but would require RhaU to isomerize a phosphorylated sugar. Some data can be interpreted as supporting the concept of RhaU functioning after phosphorylation, including the normal transport and accumulation of phosphorylated L-rhamnose in the absence of RhaU. However, the facts that *rhaU* mutants grow normally on L-rhamnose–glycerol and that unphosphorylated L-rhamnose binds to RhaU strongly suggest that RhaU functions prior to phosphorylation. Furthermore, the ability of elevated RhaK to mask the slow-growth phenotype of *rhaU* mutants is consistent with the "product pull" or displacement of the α ⇋ β equilibrium toward the β anomer by the phosphorylation step removing the β anomer from the equilibrium. Thus, RhaK must interact in some way with the ABC transporter to activate the transport of L-rhamnose, while approximately 40% of the L-rhamnose (the proportion that is β anomer) can be immediately phosphorylated by RhaK, and the mutarotation of the remaining 55 to 60% that is the α anomer is facilitated by RhaU. Whether RhaU is physically associated with RhaK and the ABC transporter has not been determined.

The structures of RhaU and the bound L-rhamnose provide important clues to how the α ⇋ β anomerization is catalyzed. The electron density of the bound L-rhamnose is well modeled as the β anomer situating OH-1 3.02 Å from Tyr20, with good geometry for hydrogen bond formation. OH-1 is also just 3.07 Å from His24, but the geometry is less ideal for hydrogen bond formation, whereas His24 is ideally situated to form a hydrogen bond with the ring O-5. In contrast, modeling shows that the α conformation would place OH-1 just 3.0 Å from the δ-CH_3 of Ile45, and 3.4 Å from Tyr20, with poor geometry for hydrogen bond formation. The initial binding of the α anomer would be facilitated by the interactions of OH-2, OH-3, OH-4, and O-5 with the protein, placing α-OH-1 in an unfavorable position from which its isomerization to the β anomer becomes an energetically favorable process. The interaction with Ile45 will force α-OH-1 to move toward Tyr20, gradually strengthening that interaction until the optimum β conformation is reached. Ring opening, in which O-5 transiently becomes an OH, is facilitated by hydrogen bonding with His24 and Trp78. The hydrogen bond with His24 provides the proton required for transient O-5-to-OH conversion as part of the sugar ring opening, and protonation of the His24 imidazole is favored by the second imidazole hydrogen bond with the main chain C═O of Tyr20, raising the imidazole pKa slightly. The hydrogen bond of O-5 with the indole of Trp78 serves to stabilize and maintain the proper orientation of O-5 and its transient OH-5 form during ring opening and closing. This reaction pathway which moves the OH-1 from a conformation with an unfavorable interaction to one with a stable hydrogen bond will be favored by 2 to 3 kcal/mol, substantially more than the ~0.2-kcal/mol barrier to anomerization.

ACKNOWLEDGMENTS

This work was supported by Discovery grants 9600 (to P.C.L.) and 238421 (to I.J.O.) from the Natural Sciences and Engineering Research Council of Canada and by the Canadian Research Chair Pro-

gram (to P.C.L.). Additional support to I.J.O. from the University of Manitoba URGP program is also acknowledged.

REFERENCES

1. **Adhya, S. L., and J. A. Shapiro.** 1969. The galactose operon of *E. coli* K-12. I. Structural and pleiotropic mutations of the operon. Genetics **62:**231–247.
2. **Altschul, S. F., T. L. Madden, A. A. Schaffer, J. Zhang, Z. Zhang, W. Miller, and D. J. Lipman.** 1997. Gapped BLAST and PSI-BLAST: a new generation of protein database search programs. Nucleic Acids Res. **25:**3389–3402.
3. **Ames, G. F.** 1986. Bacterial periplasmic transport systems: structure, mechanism, and evolution. Annu. Rev. Biochem. **55:**397–425.
4. **Baldani, J. I., R. W. Weaver, M. F. Hynes, and B. D. Eardly.** 1992. Utilization of carbon substrates, electrophoretic enzyme patterns, and symbiotic performance of plasmid-cured clover rhizobia. Appl. Environ. Microbiol. **58:**2308–2314.
5. **Beebe, J. A., A. Arabshahi, J. G. Clifton, D. Ringe, G. A. Petsko, and P. A. Frey.** 2003. Galactose mutarotase: pH dependence of enzymatic mutarotation. Biochemistry **42:**4414–4420.
6. **Beebe, J. A., and P. A. Frey.** 1998. Galactose mutarotase: purification, characterization, and investigations of two important histidine residues. Biochemistry **37:**14989–14997.
7. **Beringer, J. E.** 1974. R factor transfer in *Rhizobium leguminosarum*. J. Gen. Microbiol. **84:**188–198.
8. **Bettenbrock, K., and C.-A. Alpert.** 1998. The *gal* genes for the Leloir pathway of *Lactobacillus casei* 64H. Appl. Environ. Microbiol. **64:**2013–2019.
9. **Bouffard, G. G., K. E. Rudd, and S. L. Adhya.** 1994. Dependence of lactose metabolism upon mutarotase encoded in the *gal* operon in *Escherichia coli*. J. Mol. Biol. **244:**269–278.
10. **Dowling, D. N., and W. J. Broughton.** 1986. Competition for nodulation of legumes. Annu. Rev. Microbiol. **40:**131–157.
11. **Emsley, P., and K. Cowtan.** 2004. Coot: model-building tools for molecular graphics. Acta Crystallogr. D **60:**2126–2132.
12. **Gatz, C., J. Altschmied, and W. Hillen.** 1986. Cloning and expression of the *Acinetobacter calcoaceticus* mutarotase gene in *Escherichia coli*. J. Bacteriol. **168:**31–39.
13. **Gatz, C., and W. Hillen.** 1986. *Acinetobacter calcoaceticus* encoded mutarotase: nucleotide sequence analysis of the gene and characterization of its secretion in *Escherichia coli*. Nucleic Acids Res. **14:**4309–4323.
14. **Holden, H. M., I. Rayment, and J. B. Thoden.** 2003. Structure and function of enzymes of the Leloir pathway for galactose metabolism. J. Biol. Chem. **278:**43885–43888.
15. **Jones, J. D., and N. Gutterson.** 1987. An efficient mobilizable cosmid vector, pRK7813, and its use in a rapid method for marker exchange in *Pseudomonas fluorescens* strain HV37a. Gene **61:**299–306.
16. **Kim, M. S., J. Shin, W. Lee, H. S. Lee, and B. H. Oh.** 2003. Crystal structures of RbsD leading to the identification of cytoplasmic sugar-binding proteins with a novel folding architecture. J. Biol. Chem. **278:**28173–28180.
17. **Knee, E. M., F. C. Gong, M. Gao, M. Teplitski, A. R. Jones, A. Foxworthy, A. J. Mort, and W. D. Bauer.** 2001. Root mucilage from pea and its utilization by rhizosphere bacteria as a sole carbon source. Mol. Plant Microbe Interact. **14:**775–784.
18. **Kozlovski, V. I., L. J. Donald, V. Montero-Collado, V. Spicer, A. V. Loboda, I. V. Chernushevich, J. McNabb, W. Ens, and K. G. Standing.** 2004. Studies of noncovalent complexes of citrate synthase and catalase on a new TOF mass spectrometer with an ESI source, orthogonal injection, and 16 kV acceleration voltage. Desorption 2004, St. Petersburg, Russia.
19. **Laemmli, U. K.** 1970. Cleavage of structural proteins during the assembly of the head of bacteriophage T4. Nature **227:**680–685.
20. **McNeil, M., A. G. Darvill, S. C. Fry, and P. Albersheim.** 1984. Structure and function of the primary cell walls of plants. Annu. Rev. Biochem. **53:**625–663.
21. **Meade, H. M., S. R. Long, G. B. Ruvkun, S. E. Brown, and F. M. Ausubel.** 1982. Physical and genetic characterization of symbiotic and auxotrophic mutants of *Rhizobium meliloti* induced by transposon Tn*5* mutagenesis. J. Bacteriol. **149:**114–122.
22. **Miroux, B., and J. E. Walker.** 1996. Over-production of proteins in *Escherichia coli*: mutant hosts that allow synthesis of some membrane proteins and globular proteins at high levels. J. Mol. Biol. **260:**289–298.
23. **Murshudov, G. N., A. A. Vagin, and E. J. Dodson.** 1997. Refinement of macromolecular structures by the maximum-likelihood method. Acta Crystallogr. D **53:**240–255.
24. **Oresnik, I. J., L. A. Pacarynuk, S. A. P. O'Brien, C. K. Yost, and M. F. Hynes.** 1998. Plasmid-encoded catabolic genes in *Rhizobium leguminosaurm* bv. *trifolii:* evidence for plant-inducible L-rhamnose locus involved in competition for nodulation. Mol. Plant Microbe Interact. **11:**1175–1185.
25. **Pape, T., and T. R. Schneider.** 2004. HKL2MAP: a graphical user interface for macromolecular phasing with SHELX programs. J. Appl. Crystallogr. **37:**843–844.
26. **Perrakis, A., R. Morris, and V. Lamzin.** 1999. Automated protein model building combined with iterative structure refinement. Nat. Struct. Biol. **6:**458–463.
27. **Quandt, J., and M. F. Hynes.** 1993. Versatile suicide vectors which allow direct selection for gene replacement in gram-negative bacteria. Gene **127:**15–21.
28. **Richardson, J. S., M. F. Hynes, and I. J. Oresnik.** 2004. A genetic locus necessary for rhamnose uptake and catabolism in *Rhizobium leguminosarum* bv. trifolii. J. Bacteriol. **186:**8433–8442.
29. **Richardson, J. S., and I. J. Oresnik.** 2007. L-Rhamnose transport is sugar-kinase (RhaK) dependent in *Rhizobium leguminosarum* bv. trifolii. J. Bacteriol. **189:**8437–8446.
30. **Ryu, K. S., C. Kim, I. Kim, S. Yoo, B. S. Choi, and C. Park.** 2004. NMR application probes a novel and ubiquitous family of enzymes that alter monosaccharide configuration. J. Biol. Chem. **279:**25544–25548.
31. **Ryu, K. S., J. I. Kim, S. J. Cho, D. Park, C. Park, H. K. Cheong, J. O. Lee, and B. S. Choi.** 2005. Structural insights into the monosaccharide specificity of *Escherichia coli* rhamnose mutarotase. J. Mol. Biol. **349:**153–162.
32. **Sambrook, J., and D. W. Russell.** 2001. Moleclular cloning: a laboratory manual, 3rd ed. Cold Spring Harbor Laboratory Press, Cold Spring Harbor, NY.
33. **Sambrook, J., E. F. Fritsch, and T. A. Maniatis.** 1989. Molecular cloning: a laboratory manual, 2nd ed. Cold Spring Harbor Laboratory Press, Cold Spring Harbor, NY.
34. **Schoepfer, R.** 1993. The pRSET family of T7 promoter expression vectors for *Escherichia coli*. Gene **124:**83–85.
35. **Sheldrick, G. M.** 2002. Macromolecular phasing with SHELXE. Z. Kristallogr. **217:**644–650.
36. **Thoden, J. B., and H. M. Holden.** 2002. High resolution X-ray structure of galactose mutarotase from *Lactococcus lactis*. J. Biol. Chem. **277:**20854–20861.
37. **Thoden, J. B., J. Kim, F. M. Raushel, and H. M. Holden.** 2003. The catalytic mechanism of galactose mutarotase. Protein Sci. **12:**1051–1059.
38. **Thoden, J. B., J. Kim, F. M. Raushel, and H. M. Holden.** 2002. Structural and kinetic studies of sugar binding to galactose mutarotase from *Lactococcus lactis*. J. Biol. Chem. **277:**45458–45465.
39. **Timson, D. J., and R. J. Reece.** 2003. Identification and characterisation of human aldose 1-epimerase. FEBS Lett. **543:**21–24.
40. **Triplett, E. W., and M. J. Sadowsky.** 1992. Genetics of competition for nodulation of legumes. Annu. Rev. Microbiol. **46:**399–428.
41. **Uson, I., and G. Sheldrick.** 1999. Advances in direct methods for protein crystallography. Curr. Opin. Struct. Biol. **9:**643–648.
42. **Vincent, J. M.** 1970. A manual for the practical study of root-nodule bacteria. Blackwell Scientific Publications, Oxford, England.